An Experimental and Theoretical Study of Pyrrole Pyrolysis with Tunable Synchrotron VUV Photoionization and Molecular-Beam Mass Spectrometry

Xin Hong, Lidong Zhang, Taichang Zhang, and Fei Qi*

National Synchrotron Radiation Laboratory, University of Science and Technology of China Hefei, Anhui 230029, People's Republic of China

Received: January 12, 2009; Revised Manuscript Received: March 2, 2009

The pyrolysis of pyrrole (6.46% pyrrole in argon) has been performed with the tunable synchrotron vacuum ultraviolet (VUV) photoionization and molecular-beam mass spectrometry (MBMS) technique. The experiment was carried out over the temperature range of 1260−1710 K at a pressure of 267 Pa. About 30 intermediates have been identified by near-threshold measurements of photoionization mass spectra, and the corresponding mole fractions versus temperatures have been obtained. Moreover, the isomers of some pyrolysis products have been identified by the measurement of photoionization efficiency spectrum. The major products are H_2, C_2H_2, HCN, C_3H_4 (propyne), and C_2H_3N (acetonitrile). Meanwhile, some new intermediates, such as C_4H_4N (cyanoallyl radical) and C_2H_2N (cyanomethyl radical), have been determined. The major pyrolysis channels have been provided with the high-level ab initio G3B3 calculation and are well consistent with the experimental observation. The formation pathway of HCN via the cyclic carbene tautomer has been proved to be the lowest formation pathway, which is in accordance with previous theoretical work. The potential pathways of the early formed C_4H_4N species together with their subsequent consumption to C_2H_2N and C_2H_2 have been discussed in detail. Also, the formation pathways of the major products of C_2H_3N and C_2H_2 have been investigated as well.

1. Introduction

To reduce the emission of pollutant from the large-scale burning of nitrogen-containing fuels and coal, in addition to proper burner design, an important strategy is to use staged combustion involving a primary inert, fuel-rich reaction zone.[1] The pyrolysis study of nitrogen-containing compounds is expected to unravel the fundamental chemical reaction pathways and mechanism under these inert, fuel-rich conditions.[2] Most fuel-bound nitrogen compounds in heavy fuels are five-membered pyrrolic ring structures and six-membered pyridinic structures.

Pyrrole as a representative of pyrrolic compound, together with its isomers[3,4] and derivatives,[5−7] has been studied in the pyrolysis investigation.[8−16] The pyrolysis of pyrrole was studied behind reflected shocks in a pressurized driver single-pulse shock tube with gas chromatograph by Lifshitz et al.[9] At low temperature range, the isomers of pyrrole (allyl cyanide and *cis*-/*trans*-crotononitrile) were the principal products, together with hydrogen cyanide (HCN) and propyne/allene. At elevated temperatures, acetylene, acetonitrile, cyanoacetylene, and hydrogen became major products. Density functional theory (DFT) calculations were carried out to investigate the pathways of the unimolecular isomerization of pyrrole. It was proposed that the first step of the isomerization is a fast transition from pyrrole to pyrrolenine.[13] Another experimental and kinetics study on the pyrrole pyrolysis was investigated by Mackie et al. in a single pulse shock tube, using capillary column GC, together with GC/MS and FTIR for production identification. The determination of primary product distributions as well as the reaction rates of disappearance of reactant and of appearance of major products had also been presented. High yield of HCN implies that it is one of the major organic products. A few organic nitriles under this inert condition have also been obtained.[10] More detailed chemical kinetics analysis of pyrrole pyrolysis had been provided by ab initio calculations and by detailed chemical kinetic modeling. The reaction pathways of major products of the butenenitrile isomeric products, acetylene, acetonitrile, acrylonitrile, together with their precursor cyanoallyl radical were investigated. Also, special emphasis has been paid to the HCN and propyne formation pathway.[11]

Recently, the molecular-beam mass spectrometric technique coupled with tunable synchrotron VUV photoionization method has been applied into the experimental investigation of the pyrolysis of methyl *tert*-butyl ether (MTBE) by Zhang et al.[17,18] This method enables the unambiguous detection of intermediates, especially radicals and isomers, by reducing fragmentation via near-threshold photoionization.

In this work, the comprehensive observation of pyrolysis species has been carried out. Some new intermediates have been detected, and most isomers are identified by the measurement of photoionization efficiency spectrum. The mole fraction profiles of the major and other products are also deduced. More efforts have been put on the reaction pathways of the major products of pyrrole with the high-level ab initio G3B3 calculation. The formation pathways of C_4H_4N through H-elimination from pyrrole and the subsequent unimolecular dissociation to C_2H_2N have been provided. The formation pathways of the abundant products of HCN initiated basically from a cyclic carbine and acetonitrile (C_2H_3N) with the precursor of pyrrolenine have also been presented.

2. Experimental Method

The experiment was carried out at the National Synchrotron Radiation Laboratory (NSRL) in Hefei, China. The detail

* Corresponding author. Tel.: +86-551-3602125. Fax: +86-551-5141078. E-mail: fqi@ustc.edu.cn.

10.1021/jp9002966 CCC: $40.75
Published on Web 04/07/2009

description on the instrument setup has been reported elsewhere[17] and is briefly outlined here. An undulator radiation from the 800 MeV electron storage ring is dispersed by a 1 m Seya-Namioka monochromator with a 1500 grooves/mm laminar grating covering the photon energy range from 7.80 to 24.00 eV. The energy resolving power is approximately 1000. The average photon flux can reach the magnitude of 10^{13} photons/s. Here, a gas filter is used to eliminate higher-order harmonic radiation with Ne or Ar filled in the gas cell.[19]

In brief, the pyrolysis setup is composed of a pyrolysis chamber mounted with a high temperature furnace, a differentially pumped chamber with a molecular-beam sampling system, and a photoionization chamber with a reflection time-of-flight mass spectrometer (RTOF-MS). Pyrrole was controlled by a syringe pump (ISCO 1000D) with the liquid flow rate of 0.10 mL/min (equivalent to 0.0323 standard liter per minute (SLM) in the gas phase) at room temperature. Subsequently, pyrrole was vaporized and mixed with Ar, which was controlled by a MKS mass flow controller with the flow rate of 0.50 SLM. The vaporizer was kept at a temperature of 430 K. The mixture of pyrrole and Ar was then fed into a 3.0 mm i.d. (inside diameter) and 300 mm length alumina flow tube with 60 mm stationed inside the furnace. The pyrolysis species, including the reactant (pyrrole), intermediates, and products, were sampled by a quartz nozzle with a ~500 μm orifice at the tip. The formed molecular beam in the differentially pumped chamber then passed into the photoionization chamber through a nickel skimmer and was crossed by the tunable synchrotron VUV light. A digital delay generator (DG 535, SRS) was used to trigger a pulsed power supply and the multiscaler (P7888, FAST Comtec) as well. The ions were drawn out of the photoionization region by the pulse extraction field and subsequently collected by a microchannel plate (MCP) detector. Finally, the signal was recorded by the multiscaler via a preamplifier VT120C (EG&G, ORTEC). A silicon photodiode (SXUV-100, International Radiation Detectors, Inc.) was used to monitor the photon flux for normalizing ion signals. Pyrrole was purchased from Sinopharm Chemical Reagent Limited Co., Shanghai, China, with a purity of ≥99.5%. No further purification was performed for this study.

To reduce collisions of the pyrolysis species and detect the primary and secondary products including radicals, the pyrolysis chamber was kept at low pressure (267 Pa) in this work, which was controlled by a MKS throttle valve. The temperature was measured by a Pt-30%Rh/Pt-6%Rh thermocouple inserted in the heating region inside the flow tube. The temperature uncertainty is within 50 K.

A series of mass spectra are measured with the variation of photon energy at specified temperature for measurements of photoionization efficiency (PIE) spectra. The integrated ion intensities for a specified mass are normalized by the photon flux and then plotted as a function of the photon energy, which yields PIE spectra containing information of ionization energies (IEs) of specific species. In this work, the PIE spectra were measured at the pyrolysis temperature of 1680 K. Considering the cooling effect of molecular beam, the experimental error of determined IEs is within 0.05 eV.[20]

Mass spectra can also be recorded at fixed photon energy for various pyrolysis temperatures to yield mole fractions versus temperature. For the evaluation of mole fractions, to avoid fragmentation, mass spectra were recorded at near ionization thresholds when we scanned the temperature. In this study, the measurements of temperature scan were carried out at some selected photon energies of 16.00, 14.00, 11.80, 11.50, 11.00, 10.00, 9.50, 9.00, and 8.50 eV. The temperature range is from 1260 to 1710 K. The evaluation method of mole fraction has been reported in detail elsewhere.[17]

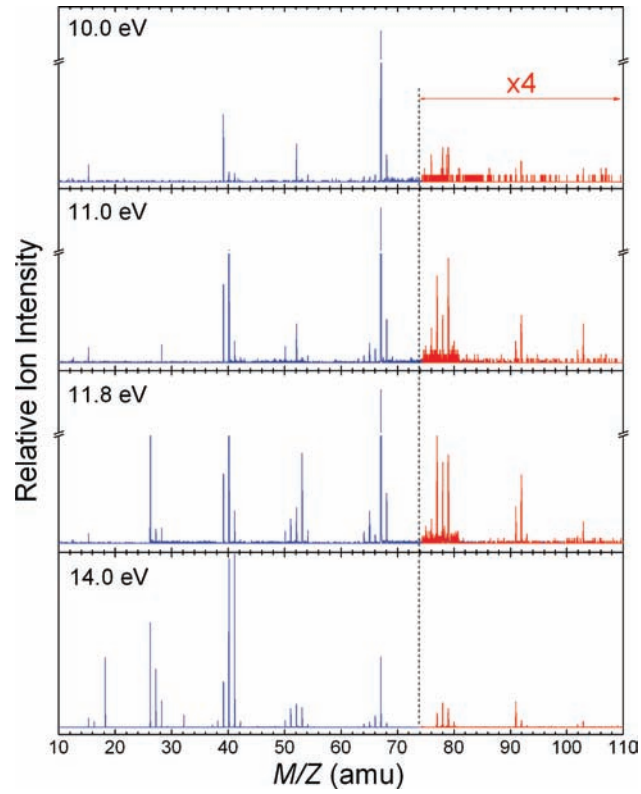

Figure 1. Photoionization mass spectra of pyrrole taken at 1680 K with four different photon energies labeled in the figure.

3. Computational Method

The highly precise calculation method G3B3[21,22] was employed to study the decomposition pathways of pyrrole. The G3B3 theory uses geometries from B3LYP/6-31G(d) and zero-point energy (ZPE) from the same level. A series of single-points energy calculations at the QCISD(T,E4T)/6-31G(d), MP4/6-31+G(d), MP4/6-31G(2df,p), and MP2(Full)/G3large levels are then carried out at the optimized geometries. It also includes a high level correction. Also, it is an approximation for the QCISD(T,E4T)/G3 large energy. All of the calculations were performed with the Gaussian 03 program.[23]

4. Results and Discussion

4.1. Identification of Pyrolysis Species. The identification of pyrolysis species is based on the measurements of photoionization mass spectra and photoionization efficiency spectra. A stack plot of photoionization mass spectra of pyrrole pyrolysis at 1680 K is presented in Figure 1 with four different photon energies ranging from 9.00 to 14.00 eV. Parts of mass spectra (from $m/z = 77$ to 120) are amplified with a factor of 4 to clearly reveal the weak peaks. Only two peaks at $m/z = 39$ and 67 can be observed at the low photon energy (9.00 eV). As the energy increased to 10.00 and 10.50 eV, the peaks become abundant, which corresponds to most of the pyrolysis intermediates and products, such as $m/z = 15$, 40, 50, 52, and trace amounts of $m/z = 64$, 65, 66, 77, 78, 79, etc. The $m/z = 28$ and $m/z = 26$ can be observed at energies of 11.00 and 11.80 eV, respectively. Some species only can be ionized by high photon energy, such as $m/z = 16$ (CH_4) and the major product $m/z = 27$ (HCN).

Furthermore, the identification of pyrolysis species can be obtained by the further measurement of PIE spectra, which have

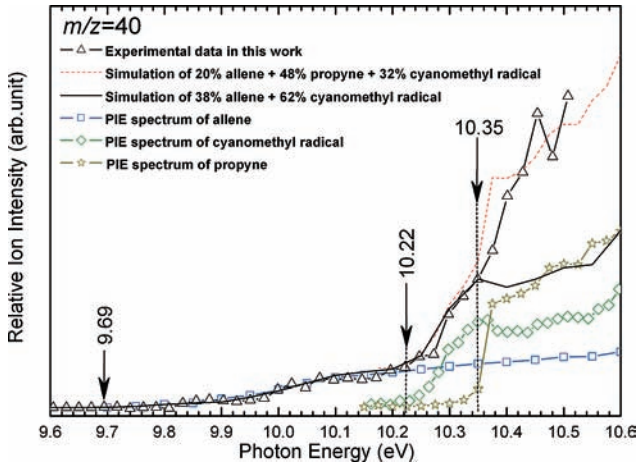

Figure 2. PIE spectrum for $m/z = 40$ (C_3H_4) measured in the pyrolysis of pyrrole. The computed simulations of relative photoionization cross sections for a mixture of 38% allene and 62% cyanomethyl radical as a dashed line and a mixture of 20% allene and 48% propyne and 32% cyanomethyl radical as a solid line are shown, respectively.

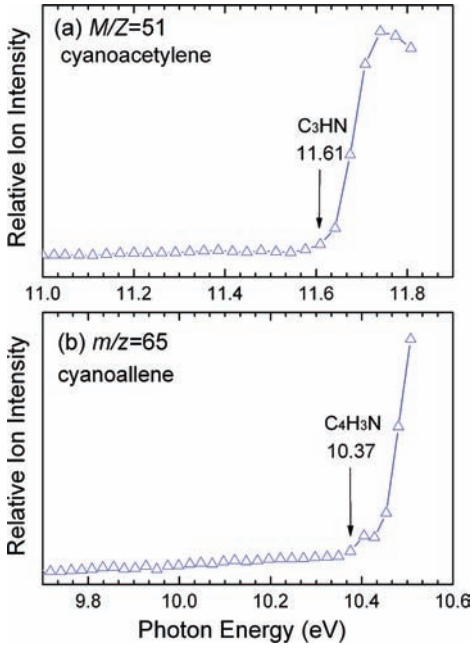

Figure 3. PIE spectra for $m/z = 51$ (C_3HN) and $m/z = 65$ (C_4H_3N) measured in the pyrolysis of pyrrole.

been selectively depicted in Figures 2 and 3. The representative PIE spectrum of $m/z = 40$ is depicted in Figure 2. Two onsets are observed at 9.69 and 10.22 eV on the PIE spectrum, which correspond to ionizations of allene (IE = 9.69 eV[24]) and cyanomethyl radical (IE = 9.9−10.9 eV[24]). However, the simulated data with various mixtures of allene and cyanomethyl radical do not fit the experimental data above 10.35 eV. Moreover, the third inflection at 10.35 eV implies existence of the third species, propyne (IE = 10.36 eV[24]). After considering contribution of pyropyne, the solid line with the isomeric composition of 20% allene, 48% propyne, and 32% cyanomethyl radical can best fit the experimental data. Similarly, clear onsets on PIE spectra of $m/z = 51$ and 65 are located at 11.61 and 10.37 eV, as shown in Figure 3a and b, which correspond to the IE of cyanoacetylene (IE = 11.62 eV[24]) and cyanoallene (IE = 10.35 eV[24]), respectively. In this work, about 30 hydrocarbon and nitrogenous intermediates and products are detected and identified, as listed in Table 1 with their IEs. For the species with trace level, their IEs are not listed in the table due to the difficulty to find clear onsets in PIE spectra.

4.2. Mole Fraction Profiles of Pyrolysis Species. A stack plot of photoionization mass spectra with the temperature range from 1260 to 1710 K is presented in Figure 4. The selected energy is 11.50 eV at which most of the pyrolysis intermediates and products can be ionized and detected. The difference can be clearly observed from the figure. Partial signals are amplified with a factor of 5 to clearly reveal the weak peaks, while the strong signal of pyrrole is divided by a factor of 5.

The mole fraction of observed pyrolysis species versus the temperature can be evaluated from measurements of near-threshold photoionization mass spectra. It should be pointed out that the photoionization cross-section data of some nitrogenous compounds are not available; fortunately, at the selected near-threshold photon energies they can be deduced from previous PIE measurements.[16,25−30] The mole fraction profiles of pyrolysis intermediates versus temperatures are shown in Figures 5 and 6. The initial formation temperatures (T_F), the maximum mole fractions (X_M), and the corresponding temperatures (T_M) of some intermediates are listed in Table 1 as well.

4.2.1. Mole Fraction Profiles of Major Pyrolysis Products. The mole fraction profiles of pyrrole and major products are displayed in Figure 5. The maximum mole fractions of hydrocarbon products (C_2H_2 and propyne) together with the nitrogenous products (HCN, C_2H_3N, and C_4H_5N) and H_2 are of the magnitude order of 10^{-2}. The concentration of HCN increases continuously as the temperature increases. The low T_F (1260 K) of HCN implies that it is one of the earliest generated species with the highest yield. The other earliest generated species is C_3H_4 (propyne) with the T_F of 1260 K and reaches its maximum concentration at 1680 K. The T_Fs of C_2H_2, C_2H_3N, and H_2 are 1350, 1410, and 1480 K, respectively. The mole fractions increase with the temperature increasing except for that of C_2H_3N.

4.2.2. Mole Fraction Profiles of Other Pyrolysis Products. The mole fraction of most hydrocarbon, nitrogenous pyrolysis intermediates and products are of the magnitude orders of 10^{-3} and 10^{-4}, as shown in Figure 6. The mole fraction profiles of C1−C3 intermediates including CH_3, CH_4, C_2H_4, C_3H_3, C_3H_4 (allene), and C_3H_3N are displayed in Figure 6a. T_Fs of these species are in the range of 1410−1450 K. Mole fractions of most intermediates increase monotonously except for that of C_3H_3, which decreases with the temperature higher than 1680 K. Figure 6b presents the mole fraction profiles of C3−C4 intermediates including C_3H_5, C_3H_6, C_4H_2, C_3HN, C_4H_4, and C_4H_6 with the T_Fs ranging from 1480 to 1600 K. The mole fraction profiles of C_4H_2, C_4H_4, and C_3HN increase continuously with temperature. However, those of C_3H_5, C_3H_6, and C_4H_6 begin to decrease around 1640 K. Figure 6c shows mole fraction profiles of C4−C6 intermediates including C_4H_3N, C_4H_4N, C_5H_4, C_5H_3N, C_5H_5N, and C_6H_6. As can be seen from the figure, T_Fs of these species are in the range of 1370−1560 K, and the T_Ms are around 1640 K with the exception of C_4H_4N, C_5H_3N, and C_6H_6. Mole fraction profiles of nitrogenous intermediates of C6−C8 together with C_7H_8 and C_8H_6 hydrocarbons are shown in Figure 6d. The T_Fs are in the range of 1410−1520 K, and the T_Ms are in the range of 1600−1680 K with an exceptive T_M of C_8H_6 at 1710 K.

The pyrolysis of pyrrole is a complex procedure; the major products together with the main pyrolysis pathways will be illustrated in detail in section 4.3. A brief discussion on the minor pyrolysis products is given as follows.

TABLE 1: Intermediates and Products Measured in the Pyrolysis of Pyrrole

			IE (eV)				
m/z	formula	species	literature[a]	this work[b]	X_M[c]	T_F (K)[d]	T_M (K)[e]
2	H_2	hydrogen	15.43	15.43	8.3×10^{-3}	1480	1710
15	CH_3	methyl radical	9.84	9.83	2.1×10^{-3}	1410	1710
16	CH_4	methane	12.61	12.60	2.6×10^{-3}	1500	1710
26	C_2H_2	acetylene	11.40	11.40	3.3×10^{-2}	1350	1710
27	HCN	hydrogen cyanide	13.60	13.60	6.0×10^{-2}	1260	1710
28	C_2H_4	ethylene	10.51	10.51	3.6×10^{-3}	1370	1710
39	C_3H_3	propargyl radical	8.67	8.65	5.8×10^{-3}	1450	1680
40	C_3H_4	allene	9.69	9.69	1.4×10^{-3}	1450	1710
	C_3H_4	propyne	10.36	10.35	1.1×10^{-2}[h]	1260[i]	1680[i]
	C_2H_2N	cyanomethyl radical	10.30	10.22			
41	C_3H_5	allyl radical	8.18	8.17	5.6×10^{-4}	1480	1660
	C_2H_3N	acetonitrile	12.20	12.20	9.7×10^{-3}	1410	1640
42	C_3H_6	propene	9.73	9.71	3.2×10^{-4}	1480	1640
50	C_4H_2	1,3-butadiyne	10.17	10.17	6.6×10^{-4}	1600	1710
51	C_3HN	cyanoacetylene	11.62	11.61	1.0×10^{-3}	1520	1710
52	C_4H_4	vinylacetylene	9.58	9.58	1.0×10^{-3}	1480	1710
53	C_3H_3N	vinylcyanide	10.91	10.91	1.0×10^{-2}	1450	1710
54	C_4H_6	1,3-butadiene	9.07	9.07	9.1×10^{-4}	1520	1640
64	C_5H_4	1,3-pentadiyne	9.50	9.50	2.0×10^{-4}	1500	1640
65	C_4H_3N	cyanoallene	10.35	10.37	2.9×10^{-4}	1450	1640
	C_5H_5	cyclopentadienyl radical	8.41	8.38			
66	C_4H_4N	cyanoallyl radical	9.18[f]	9.17	6.8×10^{-4}	<1260	1600
67	C_4H_5N	pyrrole	8.21				
77	C_5H_3N	cyanovinylacetylene	9.33	9.33	6.4×10^{-4}	1560	1710
78	C_6H_6	benzene	9.24	9.24	3.1×10^{-4}	1560	1710
79	C_5H_5N	pyridine	9.26	9.26	6.0×10^{-4}	1480	1600
91	C_6H_5N	phenylnitrene	8.0[g]		2.0×10^{-4}	1410	1600
92	C_7H_8	toluene	8.83		2.7×10^{-4}	1500	1680
102	C_8H_6	phenylacetylene	8.82	8.82	6.1×10^{-4}	1480	1710
103	C_7H_5N	benzonitrile	9.73	9.71	1.0×10^{-3}	1520	1680
117	C_8H_7N	benzeneacetonitrile	9.39		1.0×10^{-4}	1520	1680

[a] Reference 24. [b] The uncertainty for IE is 0.05 eV in this work. [c] The maximum mole fractions. [d] T_F refers to the initial temperature for formation of species. [e] T_M refers to the temperature relating to the maximum mole fraction. [f] Calculation value by highly precise G3B3. [g] Reference 34. [h] The value is total maximum mole fraction of propyne and cyanomethyl radical. [i] The value is both propyne and cyanomethyl radical.

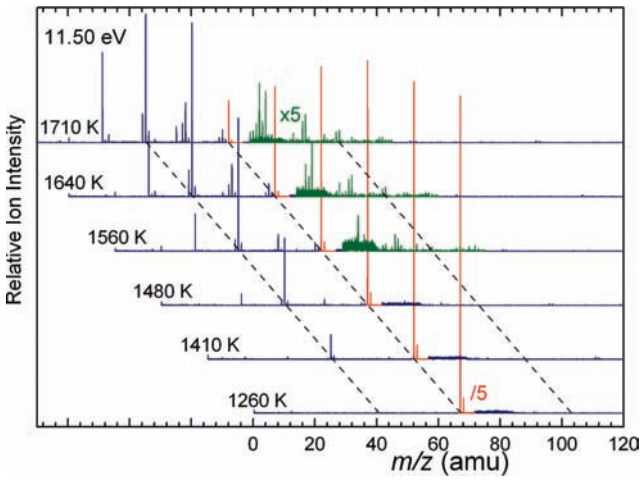

Figure 4. The stack plot of photoionization mass spectra for the pyrolysis of pyrrole with temperatures from 1260 to 1710 K at the photon energy of 11.50 eV.

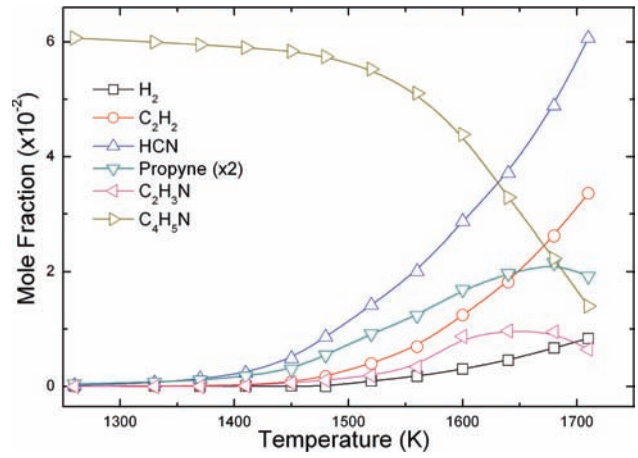

Figure 5. Mole fraction profiles for the reactant (pyrrole) and major products of the pyrolysis of pyrrole.

Vinylcyanid radical (C_3H_3N) is the most abundant among all detected intermediates. The production of methyl radical and vinylcyanid radical may be derived mostly from the decomposition of crotonitrile.[6] Both radicals can undergo the H abstraction process yielding methane and vinylcyanide, respectively. The vinylcyanide can also be formed directly by H attack to the crotonitrile with the counterpart methyl radical.[11] The profile of the methyl radical is consistent with that of vinylcyanide, but much different in concentration at higher temperature. The formation of methane is correlative to this variance. The minor amount of ethylene (C_2H_4) originates from the H attack to allyl cyanide. According to the previous theoretical calculation by Mackie et al., the pyrolysis of a cyclic carbene with the energy barrier of 82 kcal/mol with G2(MP2) method contributes much to the formation of allene.[11] According to the consumption pathway proposed by Lifshitz et al.,[9] methane is a major product in the pyrolysis of propyne, whereas allene is a precursor to ethylene. Yet the T_F of C_2H_4 at 1370 K, which is lower than the T_F of allene at 1450 K, rules out this as the main formation

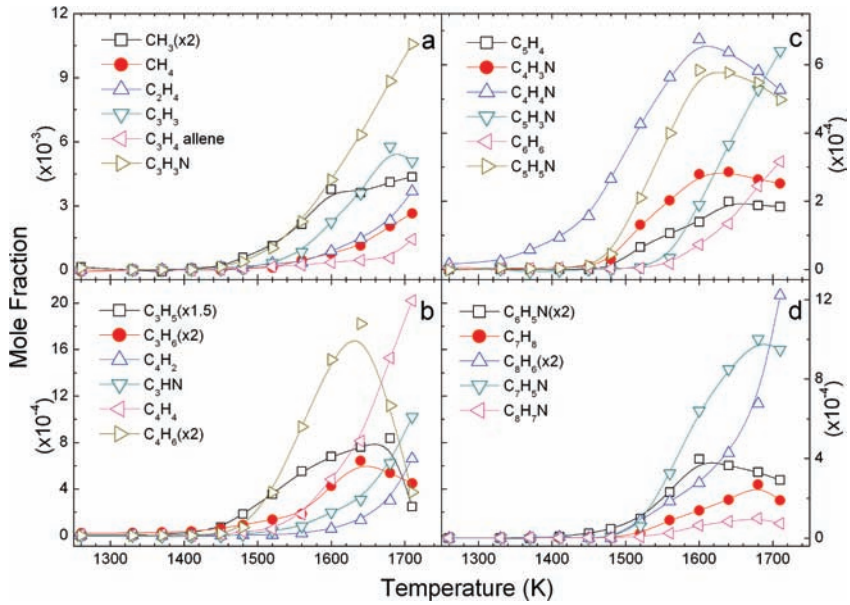

Figure 6. Mole fraction profiles for the other pyrolysis intermediates and products of pyrrole.

pathway. With respect to the result of Mackie et al., the free radical mechanism of the H attack to the allyl cyanide is the main source of C_2H_4.[11] The attack of the methyl radical to propyne produces the methane and C_3H_3. The decreasing profile tendencies of the methyl radical interpret the conversion of methane well.

The above-mentioned cyanovinyl radical can easily form vinylcyanide either by abstraction or by recombination with a hydrogen atom and cyanoacetylene by the loss of a hydrogen atom. The C4 species, 1,3-butadiyne (C_4H_2), vinylacetylene (C_4H_4), and 1,3-butadiene (C_4H_6), are detected and formed in accordance with the proposed radical reactions proposed by Mackie et al.[10,11] Propene (C_3H_6) is formed at nearly the same temperature with allyl radical (C_3H_5), but has lower concentration. C_3H_5 is produced from the reaction of H atom and allyl cyanide with the formation of HCN, while at high temperature, C_3H_5 would be consumed by decomposition to propyne and H atom, which can be reflected on the descendant profile of C_3H_5.

According to the theoretical study summarized by Lifshitz et al., the production of HCN from the unsaturated organic nitriles is indeed the main reaction. Yet the production of molecular hydrogen and the counterpart cyanoallene should be present as well.[6] These compounds appear only at high temperature and in trace quantities, which is in accordance with the mole fraction profile of C_4H_3N. Benzene is a minor product at high temperature. The C_3H_3 radical, which is mainly produced by an abstraction of a hydrogen atom from both allene and propyne, can dimerize for the formation of benzene. The other species including C_5H_3N and C_5H_5N in Figure 6c are derived from the rearrangement of secondary pyrolysis products. C_5H_3N and C_5H_5N are identified as cyanovinylacetylene and pyridine, respectively.

C_6H_5N is recognized as phenylnitrene (PhN), which has also been detected in the rich pyrrole flame.[31] C_7H_5N together with C_7H_8 and C_8H_7N are benzonitrile, toluene, and benzeneacetonitrile, respectively. The profiles of the above-mentioned four species in Figure 6d are formed with the same tendency. The distinct profile of C_8H_6 is identified as phenylacetylene, which increases sharply at higher level of pyrolysis.

4.3. Major Pyrolysis Pathways. The major reaction pathways include the tautomerism of pyrrole, ring-opening, and the

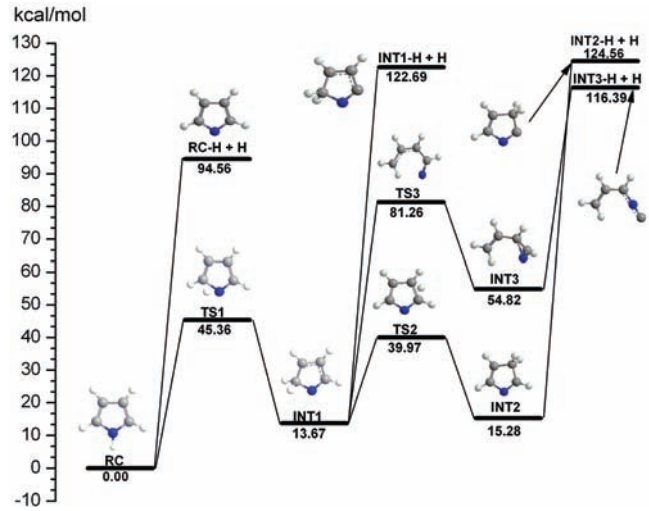

Figure 7. Relative energies of automatizms and H-elimination reactions involved in the pyrolysis of pyrrole at the G3B3 level of theory. Energies are relative to **RC**.

decomposition reactions. At lower temperature, pyrrolenines (2H-pyrrole **INT1**, 3H-pyrrole **INT2**, as shown in Figure 7), butenenitrile, allyl cyanide, and *cis*-/*trans*-crotononitrile ($CH_3CHCHCN$) can be formed via tautomerism and ring-opening reactions. HCN and C_3H_4 (propyne) appear to be the primary products as well. HCN, acetonitrile, and propyne are also formed at low temperature with high concentration. As temperature increases, acetylene, allene, and other products become increasingly important products.

Pyrrole is known to rearrange thermally at temperature between 773 and 873 K, and tautomerization reaction initiates pyrolysis process.[32] Mackie et al.[10,11] postulated that pyrolysis procedure was initiated most readily by the lowest pathway of the reversible formation of pyrrolenines, among which 2H-pyrrole has been detected by Tian et al. in the premixed pyrrole flames.[33] The following ring scission forms an open chain biradical intermediate, which will readily undergo hydrogen transfer reaction to form two highly stable butenenitrile isomers of pyrrole, *cis*-crotononitrile and allyl cyanide. The active energies for the formation of 2H- and 3H-pyrrole are lower

TABLE 2: The Proposed Major Reactions for Pyrrole Pyrolysis

Reactions	Reaction Styles
C_4H_5N(**RC**) → 2H-pyrrole (**INT1**)	Tautomerization reactions
RC → cyclic carbine (**INT4**)	
INT1 → 3H-pyrrole (**INT2**)	
INT1 → open ring biradical (**INT3**)	
INT1 → cis-/trans-C_3H_5N	
INT1 → allyl cyanide (**INT12**)	
RC → **RC**-H + H	H-elimination reactions
INT1 → **INT1**-H +H	
INT2 → **INT2**-H +H	
INT3 → **INT3**-H +H	
RC → **INT4** → HCN + CH_3CCH	HCN + C_3H_4 formation pathways
RC → **INT1** → HCN + C_3H_4	
RC → **INT2** → HCN + C_3H_4	
RC-H → CHNCH + C_2H_2	C_2H_2N + C_2H_2 formation pathways
INT1-H → CH_2NC + C_2H_2	
INT2-H → CH_2CN + C_2H_2	
INT3-H → CH_2NC + C_2H_2	
INT1 → CH_2NCH + C_2H_2	C_2H_3N + C_2H_2 formation pathways
INT1 → CH_2CNH + C_2H_2	
INT1 → CH_3CN + C_2H_2	

according to the calculations of Mackie et al. at G2(MP2) level,[11] whereas the other carbene tautomers are less stable and the corresponding energy barriers are higher. Comparing the formation of pyrrolenines, the ring-opening reactions do not readily happen, because it is difficult for the fission of the C−C or C−N bond. Some ring-opening species are the precursors of the decomposition products. In general, thermal decomposition is preceded by the ring-opening process. It can be reasonably assumed that isomers of pyrrole contribute to the early step of pyrrole pyrolysis, which is consistent with the previous experimental results.[9,10] In this Article, the primary products are mainly the further pyrolysis products from the proposed isomeric intermediates, pyrrolenines. Some major pyrolysis pathways are discussed in detail as follows, which are also listed in Table 2.

4.3.1. C_4H_4N Formation Pathways. C_4H_4N is one of the most important species and has been identified in this work. It exists in the early stage of the pyrolysis with T_F lower than 1260 K, as shown in Figure 6c. Direct cleavage of C−H bonds of **RC** can occur at different positions. The corresponding cleavage energies are 118.60 and 119.10 kcal/mol, whereas the cleavage energy of N−H bond is lower, which is 94.56 kcal/mol, and thus the formation of C_4H_4N is mainly initiated from the hydrogen elimination of **RC**, as shown in Figure 7. The pyrrolenines (**INT1** and **INT2**) can also form C_4H_4N through direct H-elimination reaction except in the form of **RC**−**H**. The C−H bond fission of **INT1** can occur at three different positions with the relevant energies of 122.69, 130.45, and 130.51 kcal/mol. The **INT1** can also further transform to **INT2** and **INT3** via the corresponding transition states **TS2** and **TS3** as shown in Figure 7. For **INT2**, there are three ways of C−H bond fission with the respective energies of 124.56, 130.95, and 133.19 kcal/mol. When it comes to the open ring biradical **INT3,** there are four products of H-elimination with the energies of 116.39, 130.56, 147.77, and 165.57 kcal/mol, respectively. Among them, the **INT1**−**H** and **INT3**−**H** are relatively lower in energy with the calculated dissociation energies of 122.69 and 116.39 kcal/mol. The structures of the C_4H_4N and the corresponding bond scission energies have been listed in Table 3. Also, the relative energies of tautomerism and H-elimination reactions involved in the pyrolysis of pyrrole at the G3B3 level have been clearly depicted in Figure 7.

TABLE 3: H-Elimination Products and Relative Energies from RC, INT1, INT2, and INT3

Precursors	Product structures	Bond scission energies (kcal/mol)
RC		94.561
		118.60
		119.10
INT1		122.69
		130.45
		130.51
INT2		124.56
		130.95
		133.19
INT3		116.39
	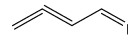	130.56
	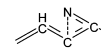	147.77
	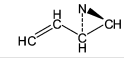	165.57

The free radical mechanism of the H atom attacking to pyrrole also contributes to the formation of C_4H_4N together with H_2 formation. The experimental measurement shows the T_F of H_2 at 1480 K, which much differs from the T_F of C_4H_4N. Thus, this mechanism can be ruled out as the major one at lower temperature.

4.3.2. HCN + C_3H_4 Formation Pathways. HCN is the most abundant product formed at low pyrolysis temperature. There are different pathways to form HCN and C_3H_4. According to previous ab initio calculations, the tautomerism or ring-opening steps are the rate-determining steps. The reaction pyrrole (**RC**) → **INT4** → HCN + C_3H_4 via the cyclic carbene tautomer **INT4** is the lowest energy pathway. The G3B3 calculation results are shown in Figure 8. The calculated results for the formation pathways of HCN + C_3H_4 are in good accordance with previous theoretical work at CASSCF, CASPT2, and G2(MP2) levels.[11] The pathway involves the tautomerism of pyrrole to a cyclic carbene (**INT4**) undergoing a transition state (**TS4**) with an energy barrier of 72.23 kcal/mol. The energy barrier of the following ring-opening reaction is very low (7.17 kcal/mol, **TS5**). Next, the HCN and propyne (CH_3CCH) are formed through the hydrogen rotation and migration. In this reaction, the tautomerism reaction is the rate-determining step with an energy barrier of 72.23 kcal/mol. This is constant with our experimental measurement, of which the T_Fs of the two primary products are both at 1260 K.

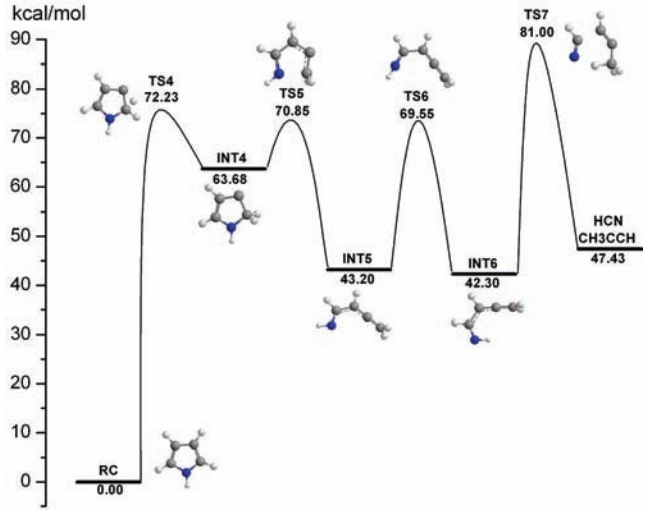

Figure 8. Relative energies of one possible formation pathway of HCN + C_3H_4 involved in the pyrolysis of pyrrole at the G3B3 level of theory. Energies are relative to **RC**.

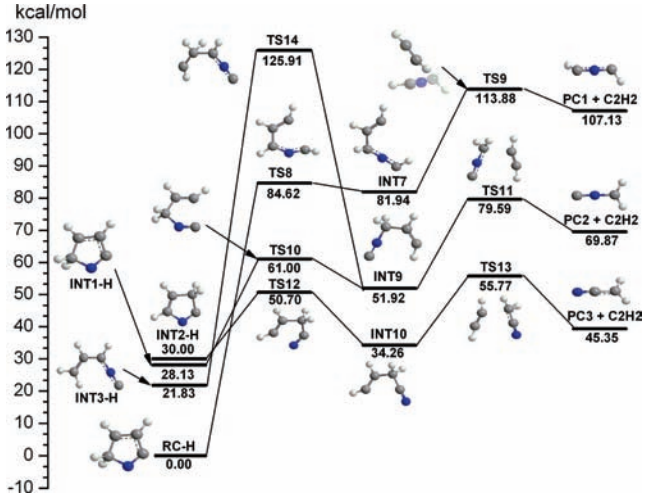

Figure 9. Relative energies of $C_4H_4N \rightarrow C_2H_2N + C_2H_2$ reaction pathways involved in the pyrolysis of pyrrole at the G3B3 level of theory. Energies are relative to **RC**−**H**.

The pyrrolenines (2H-pyrrole **INT1**, 3H-pyrrole **INT2**), butenenitrile, allyl cyanide, and *cis*-/*trans*-crotononitrile can also decompose to HCN and C_3H_4 with the higher energy barriers. At high temperature, these reactions may also contribute to the formation of HCN and C_3H_4. Apart from the above-mentioned formation pathways of C_3H_4 (propyne), H abstraction of allyl radical may also contribute to the propyne formation.

4.3.3. $C_2H_2N + C_2H_2$ Formation Pathways from C_4H_4N. The subsequent consumption pathways of C_4H_4N to C_2H_2N and C_2H_2, depicted in Figure 9, can explain the existence of C_4H_4N with relatively low concentration. As proposed above, for the facile H-elimination from **RC**, pyrrolenines such as 2H-pyrrole (**INT1**), 3H-pyrrole (**INT2**), and the open ring biradical (**INT3**) are all proposed precursors for the production of C_2H_2N and C_2H_2.

RC−**H** as the main C_4H_4N product can further decompose to C_2H_2N (**PC1**) and C_2H_2. In this reaction, the ring-opening reaction to unstable **INT7** via transition state (**TS8**) is the rate-determining step. The energy barrier is 84.62 kcal/mol. The C−C bond cleavage and the unstable C_2H_2N (**PC1**) are then formed overcoming a relative low energy barrier of 31.94 kcal/mol. The H-elimination product of **INT1**−**H** will

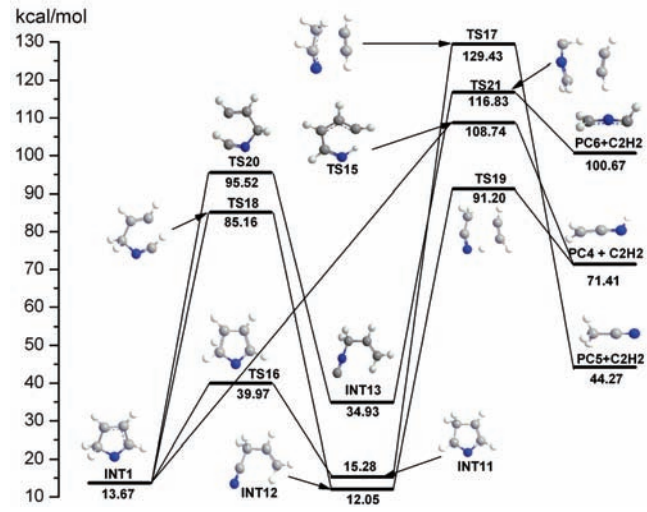

Figure 10. Relative energies of **INT1** $\rightarrow$ $C_2H_3N + C_2H_2$ reaction pathways involved in the pyrolysis of pyrrole at the G3B3 level of theory. Energies are relative to **RC**.

further undergo a low energy barrier of 32.87 kcal/mol with the formation of **INT9**. Next is the decomposition of **INT9** to C_2H_2N (**PC2**) and C_2H_2 surmounting an energy barrier of 27.67 kcal/mol. The H-elimination pathway of **INT3** has a lower dissociation energy (61.57 kcal/mol). The relatively more stable **INT3**−**H** can also form **INT9** though H migration. Yet the corresponding energy barrier is higher (104.08 kcal/mol). The **INT2**−**H** radical is unstable and will overcome a low relative energy barrier of 20.70 kcal/mol (**TS12**) and will undergo the subsequent dissociation pathway mounting a low energy barrier of 21.51 kcal/mol with the production of C_2H_2N (**PC3**) and C_2H_2. This is the main pathway with the lowest energy barrier for the production of C_2H_2N and C_2H_2.

The formed C_2H_2N is unstable and can produce acetonitrile (CH_3CN) by H addition. The readily conversion of C_2H_2N can explain the low concentration of C_2H_2N. It can be concluded that it is the most sensitive reaction for the formation of C_2H_2N, C_2H_2, and C_2H_3N with respect to the low energy barrier, which is in accordance with previous study.[11]

4.3.4. $C_2H_3N + C_2H_2$ Formation Pathways. As temperature increases, acetylene becomes an increasingly important product whose concentration exceeds that of propyne. The formations of $C_2H_3N + C_2H_2$ have many different pathways. In this work, we studied the formations of $C_2H_3N + C_2H_2$ from **INT1** with the G3B3 method, as shown in Figure 10.

There are four pathways considered in this study (Figure 11). (1) The 2H-pyrrole (**INT1**) can isomerize to 3H-pyrrole (**INT11**) with an energy barrier of 26.30 kcal/mol, following the dissociation via **TS17** to C_2H_3N (**PC5**) and C_2H_2 with an energy barrier of 114.15 kcal/mol. This reaction includes the C−C bond cleavage and H migration. (2) The direct ring-opening biradical of the 2H-pyrrole (**INT1**) can decompose to C_2H_3N and C_2H_2 with an energy barrier of 95.07 kcal/mol (**TS15**), which constitutes another assumed potential formation pathway of C_2H_3N (**PC4**) and C_2H_2. Yet **PC4** is unstable and 27.14 kcal/mol higher in energy than **PC5**. It is a reasonably important reaction in the pyrolysis procedure at least at higher temperature, which is consistent with a previous study.[11] (3) The allyl cyanide (**INT12**) is more stable than **INT1**, which is 1.61 kcal/mol lower in energy. Also, **INT12** is derived from **INT1** via the transition state (**TS18**) with an energy barrier of 71.49 kcal/mol. It can readily

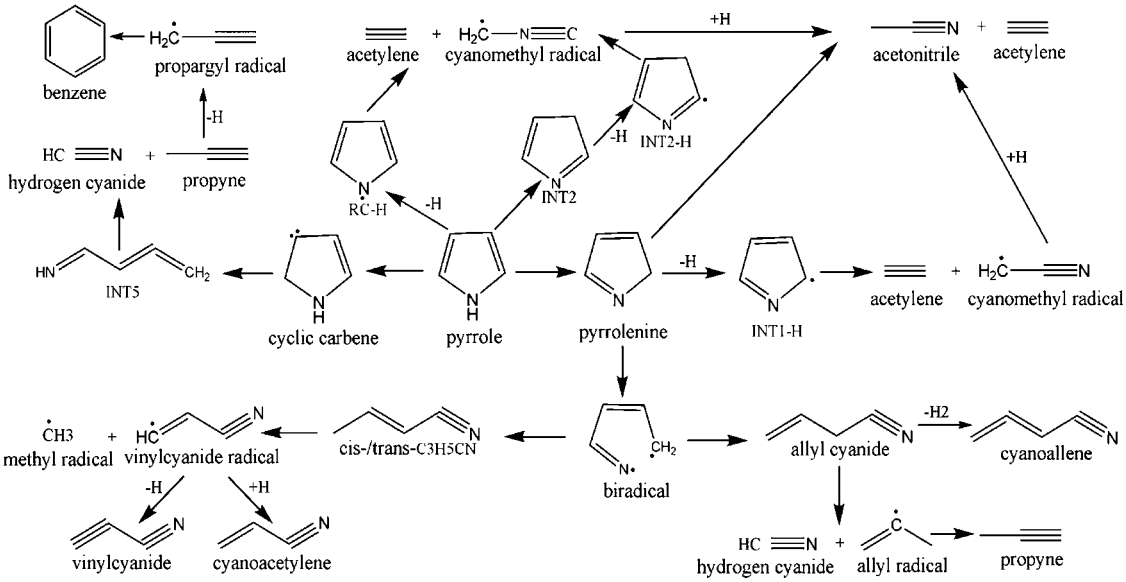

Figure 11. A schematic network of pyrrole transformation in the pyrolysis process at temperatures from 1260 to 1710 K.

undergo a C−C dissociation to form C_2H_3N (**PC4**) and C_2H_2 via transition state **TS19** with an energy barrier of 79.15 kcal/mol. (4) The 1,4 H-transfer of **INT1** via **TS20** will engender allyl isocyanide (**INT13**) with an energy barrier of 81.85 kcal/mol. Next, C_2H_3N (**PC6**) and C_2H_2 are formed surmounting an energy barrier of 81.90 kcal/mol. The products **PC6** and **PC4** will isomerize to acetonitrile (**PC5**). This can explain the difference of T_Fs of the counterparts (T_F of C_2H_2 at 1350 K, and T_F of C_2H_3N at 1410 K).

5. Conclusion

The pyrrole pyrolysis has been studied with the tunable synchrotron VUV photoionization and molecular-beam mass spectrometry combined with theoretical calculations. Isomers of intermediates have been identified with measurements of photoionization efficiency spectra and photoionization mass spectra, and mole fractions are obtained by scanning the pyrolysis temperature at selective photon energies near ionization threshold. The detailed formation pathways of major products such as C_4H_4N, C_2H_2N, C_2H_3N, C_2H_2, HCN, and C_3H_4 (propyne) have been calculated with the highly precise G3B3 method, and the lowest formation pathways of each product have been depicted. As compared to previous investigations, more pyrolysis species have been detected in this work, especially identification of radicals and isomers. Trace amounts of secondary pyrolysis intermediates and a few C5−C8 recombination species have also been detected with low concentration at high temperature.

On one hand, the thermal decomposition of C_4H_4N from the H-elimination of pyrrole is the lowest formation pathway of C_2H_2N. On the other hand, pyrrole can also readily undergo tautomerization to form pyrrolenines prior to any other thermal decomposition procedure. The subsequent ring-opening reactions of pyrrolenines, biradical, and the butenenitrile isomers are the precursors of the pyrolysis products. HCN and propyne arise principally from a cyclic carbene with the lowest energy barrier. Although highly precise computations performed in this work enrich the high temperature chemistry of pyrolysis process, further efforts are desired in investigating reaction rate constants of the pyrolysis pathways and in developing a detailed kinetic modeling study.

Acknowledgment. F.Q. is grateful for funding support from the Chinese Academy of Sciences, Natural Science Foundation of China under Grant no. 20533040, National Basic Research Program of China (973) under Grant no. 2007CB815204, and Ministry of Science and Technology of China under Grant no. 2007DFA61310.

References and Notes

(1) Axworthy, A. E.; Dayan, V. H.; Martin, G. B. *Fuel* **1978**, *57*, 29.
(2) Nelson, P. F.; Buckley, A. N.; Kelly, M. D. *Proc. Combust. Inst.* **1992**, *24*, 1259.
(3) Butler, J. N.; Mcalpine, R. D. *Can. J. Chem.* **1963**, *41*, 2487.
(4) Doughty, A.; Mackie, J. C. *J. Chem. Phys.* **1992**, *96*, 272.
(5) Patterson, J. M.; Soedigdo, S. *J. Org. Chem.* **1968**, *33*, 2057.
(6) Lifshitz, A.; Bidani, M.; Suslensky, A.; Tamburu, C. *J. Phys. Chem.* **1989**, *93*, 1369.
(7) Sendt, K.; Ikeda, E.; Bacskay, G. B.; Mackie, J. C. *J. Phys. Chem. A* **1999**, *103*, 1054.
(8) Bruinsma, O. S. L.; Tromp, P. J. J.; de Sauvage Nolting, H. J. J.; Montijn, J. A. *Fuel* **1988**, *67*, 334.
(9) Lifshitz, A.; Tamburu, C.; Suslensky, A. *J. Phys. Chem.* **1989**, *93*, 5802.
(10) Mackie, J. C.; Colket, P. F.; Nelson, P. F.; Esler, M. *Int. J. Chem. Kinet.* **1991**, *23*, 733.
(11) Martoprawiro, M.; Bacskay, G. B.; Mackie, J. C. *J. Phys. Chem. A* **1999**, *103*, 3923.
(12) Lei, Z.; Xuefeng, Z.; Ruifeng, L. *J. Phys. Chem. A* **1999**, *103*, 3917.
(13) Dubnikova, F.; Lifshitz, A. *J. Phys. Chem. A* **1998**, *102*, 10880.
(14) Oh, C. Y.; Choi, H.; Kim, H. L. *Int. J. Quantum Chem.* **2007**, *107*, 92.
(15) Bacskay, G. B.; Martoprawiro, M.; Mackie, J. C. *Chem. Phys. Lett.* **1999**, *300*, 321.
(16) Thorn, R. P.; Monks, P. S.; Stief, L. J.; Kuo, S. C.; Zhang, Z. Y.; Ross, S. K.; Klemm, R. B. *J. Phys. Chem. A* **1998**, *102*, 846.
(17) Zhang, T. C.; Wang, J.; Yuan, T.; Hong, X.; Zhang, L. D.; Qi, F. *J. Phys. Chem. A* **2008**, *112*, 10487.
(18) Zhang, T. C.; Zhang, L. D.; Wang, J.; Yuan, T.; Hong, X.; Qi, F. *J. Phys. Chem. A* **2008**, *112*, 10495.
(19) Zhang, T. C.; Zhu, A. G.; Hong, X.; Pan, Y.; Shan, X. B.; Sheng, L. S.; Zhang, Y. W.; Qi, F. *J. China Univ. Sci. Technol.* **2007**, *37*, 582.
(20) Kamphus, M.; Liu, N. N.; Atakan, B.; Qi, F.; Mcllroy, A. *Proc. Combust. Inst.* **2002**, *29*, 2627.
(21) Baboul, A. G.; Curtiss, L. A.; Redfern, P. C.; Raghavachari, K. *J. Chem. Phys.* **1999**, *110*, 7650.
(22) Curtiss, L. A.; Raghavachari, K.; Redfern, P. C.; Rassolov, V.; Pople, J. A. *J. Chem. Phys.* **1998**, *109*, 7764.
(23) Frisch, M. J.; Trucks, G. W.; Schlegel, H. B.; Scuseria, G. E.; Robb, M. A.; Cheeseman, J. R.; Zakrzewski, V. G.; Montgomery, J. A., Jr.; Stratmann, R. E.; Burant, J. C.; Dapprich, S.; Millam, J. M.; Daniels, A. D.; Kudin, K. N.; Strain, M. C.; Farkas, O.; Tomasi, J.; Barone, V.; Cossi, M.; Cammi, R.; Munnucci, B.; Pomelli, C.; Adamo, C.; Clliford, S.; Ochterski,

J.; Petersson, G. A.; Ayala, P. Y.; Cui, Q.; Morokuma, K.; Rega, N.; Salvador, P.; Dannenberg, J. J.; Malick, D. K.; Rabuck, A. D.; Raghavachari, K.; Foresman, J. B.; Cioslowski, J.; Ortiz, J. V.; Baboul, A. G.; Stefanov, B. B.; Liu, G.; Liashenko, A.; Pikorz, P.; Komaromi, I.; Gomperts, R.; Martin, R. L.; Fox, D. J.; Keith, T.; Al-Laham, M. A.; Peng, C. Y.; Nakayakkara, A.; Challacombe, M.; Gill, P. M. W.; Johnson, B.; Chen, W.; Wong, M. W.; Andres, J. L.; Gonzalez, C.; Challacombe, M.; Gill, P. M. W.; Johnson, B.; Chen, W.; Wong, M. W.; Andres, J. L.; Gonzales, C.; Head-Gordon, M.; Replogle, E. S.; Pople, J. A. *Gaussian 03*, revision C.02; Gaussian, Inc.: Wallingford, CT, 2004.

(24) Linstrom, P. J.; Mallard, W. G. *NIST Chemistry Webbook*; National Institute of Standard and Technology, 2005.

(25) Cool, T. A.; Nakajima, K.; Mostefaoui, T. A.; Qi, F.; McIlroy, A.; Westmoreland, P. R.; Law, M. E.; Poisson, L.; Peterka, D. S.; Ahmed, M. *J. Chem. Phys.* **2003**, *119*, 8356.

(26) Wirsich, J. *Spectrosc. Lett.* **1990**, *23*, 741.

(27) Rider, D. M.; Ray, G. W.; Darland, E. J.; Leroi, G. E. *J. Chem. Phys.* **1981**, *74*, 1652.

(28) Schwell, M.; Jochims, H.-W.; Baumgartel, H.; Leach, S. *Chem. Phys.* **2008**, *344*, 164.

(29) Kreile, J.; Kurland, H. D.; Seibel, W.; Schweig, A. *Chem. Phys.* **1991**, *155*, 99.

(30) Kanno, N.; Tonokura, K. *Appl. Spectrosc.* **2007**, *61*, 896.

(31) Tian, Z. Y.; Li, Y. Y.; Zhang, T. C.; Zhu, A. G.; Qi, F. *Chin. J. Chem. Phys.* **2007**, *20*, 425.

(32) Rendall, W. A.; Torres, M.; Lown, E. M.; Strause, O. P. *Rev. Chem. Intermed.* **1986**, *6*, 335.

(33) Tian, Z. Y.; Li, Y. Y.; Zhang, T. C.; Zhu, A. G.; Cui, Z. F.; Qi, F. *Combust. Flame* **2007**, *151*, 347.

(34) Che, H.; Bi, H.; Ding, R.; Wang, D.; Meng, L.; Zheng, S.; Wang, D.; Mok, K. W.; Chau, F. T. *Chem. Phys. Lett.* **2003**, *382*, 291.

JP9002966